Plasmonic Light Trapping in Thin-film Silicon Solar Cells with Improved Self-Assembled Silver Nanoparticles

ARTICLE *in* NANO LETTERS · JUNE 2012

Impact Factor: 13.59 · DOI: 10.1021/nl301521z · Source: PubMed

4 AUTHORS, INCLUDING:

Hairen Tan
University of Toronto
33 PUBLICATIONS **615** CITATIONS
SEE PROFILE

Arno H. M. Smets
Delft University of Technology
117 PUBLICATIONS **1,349** CITATIONS
SEE PROFILE

Miro Zeman
Delft University of Technology
277 PUBLICATIONS **2,740** CITATIONS
SEE PROFILE

NANO LETTERS

Letter

pubs.acs.org/NanoLett

Plasmonic Light Trapping in Thin-film Silicon Solar Cells with Improved Self-Assembled Silver Nanoparticles

Hairen Tan,* Rudi Santbergen, Arno H. M. Smets, and Miro Zeman

Photovoltaic Materials and Devices Laboratory, Delft University of Technology, P.O. Box 5031, 2600 GA Delft, The Netherlands

Supporting Information

ABSTRACT: Plasmonic metal nanoparticles are of great interest for light trapping in thin-film silicon solar cells. In this Letter, we demonstrate experimentally that a back reflector with plasmonic Ag nanoparticles can provide light-trapping performance comparable to state-of-the-art random textures in n-i-p amorphous silicon solar cells. This conclusion is based on the comparison to high performance n-i-p solar cell and state-of-the-art efficiency p-i-n solar cells deposited on the Asahi VU-type glass. With the plasmonic back reflector a gain of 2 mA/cm^2 in short-circuit current density was obtained without any deterioration of open circuit voltage or fill factor compared to the solar cell on a flat back reflector. The excellent light trapping is a result of strong light scattering and low parasitic absorption of self-assembled Ag nanoparticles embedded in the back reflector. The plasmonic back reflector provides a high degree of light trapping with a haze in reflection greater than 80% throughout the wavelength range 520−1100 nm. The high performance of plasmonic back reflector is attributed to improvements in the self-assembly technique, which result in a lower surface coverage and fewer small and irregular nanoparticles.

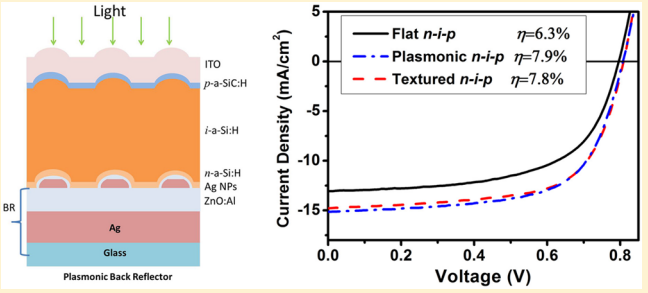

KEYWORDS: *Light trapping, plasmonics, back reflector, photovoltaics, thin-film silicon solar cells*

Advanced light trapping concepts are crucial to achieve high-efficiency thin-film silicon (TF-Si) solar cells due to the low absorption coefficient of silicon in the near-infrared region. Light scattering at randomly textured interfaces is currently the standard light trapping scheme and has resulted in state-of-the-art efficiency of TF-Si solar cells.[1−6] In the past few years, subwavelength plasmonic metal nanoparticles have attracted much attention for effective light trapping because they can induce localized surface plasmons and strongly scatter incident light into the absorber layers, thereby increasing the average light path length inside solar cells.[7−11] The optical properties of metal nanoparticles are sensitive to their size, shape, surface coverage on the substrate, surrounding medium, and so forth.[11−15] The light can be either scattered or absorbed by metal nanoparticles.[12,15] Therefore, the metal nanoparticles must be well designed to maximize the scattering and to minimize absorption across the wavelength range of interest in solar cells. Silver nanoparticles (Ag NPs) are commonly used because of their large scattering cross-section and potential for low absorption in the visible and near-infrared spectrum.[11,15]

Metal nanoparticles placed on front or rear sides of a solar cell can lead to preferential scattering of light into the semiconductor layers. However, metal nanoparticles are better to be placed at the rear side to avoid the suppression of photocurrent at wavelengths below the surface plasmon resonance.[16−19] In TF-Si solar cells the metal nanoparticles can be embedded in the back reflector and scatter the incident light that is not absorbed during the first pass. Moulin et al. and Eminian et al. demonstrated that the Ag/ZnO back reflector (BR) with random arrays of Ag NPs could significantly enhance the photocurrent in n-i-p hydrogenated amorphous Si (a-Si:H) and microcrystalline Si (μc-Si:H) solar cells compared to cells on the flat BR without Ag NPs due to the strong scattering of Ag NPs.[20−22] We refer to the back reflector with Ag NPs as a plasmonic BR. Recently, the plasmonic BR has also been shown to exceed the moderately randomly textured BR in μc-Si:H solar cells, where the textured BR has similar roughness as the plasmonic BR.[23] However, the achieved light-trapping capacity of the plasmonic BRs in those solar cells is all below that can be achieved by state-of-the-art random textures used in the same type TF-Si solar cells.

In the meantime, periodically patterned plasmonic back contacts have been implemented in TF-Si solar cells, in which the light absorption can be improved by coupling the incident light into waveguide modes or surface plasmon polaritons modes.[24−29] Ferry et al. designed nanopatterned Ag/ZnO plasmonic BR by nanoimprint lithography and showed that the nanopatterned plasmonic BR resulted in better light trapping than Asahi U-type glass in ultrathin a-Si:H solar cells, where the thickness of intrinsic a-Si:H layer (i-layer) is no more than 160 nm.[24−26] However, the spectral response of such ultrathin plasmonic solar cells is far below that of a-Si:H solar cell with

Received: April 23, 2012
Revised: June 21, 2012
Published: June 27, 2012

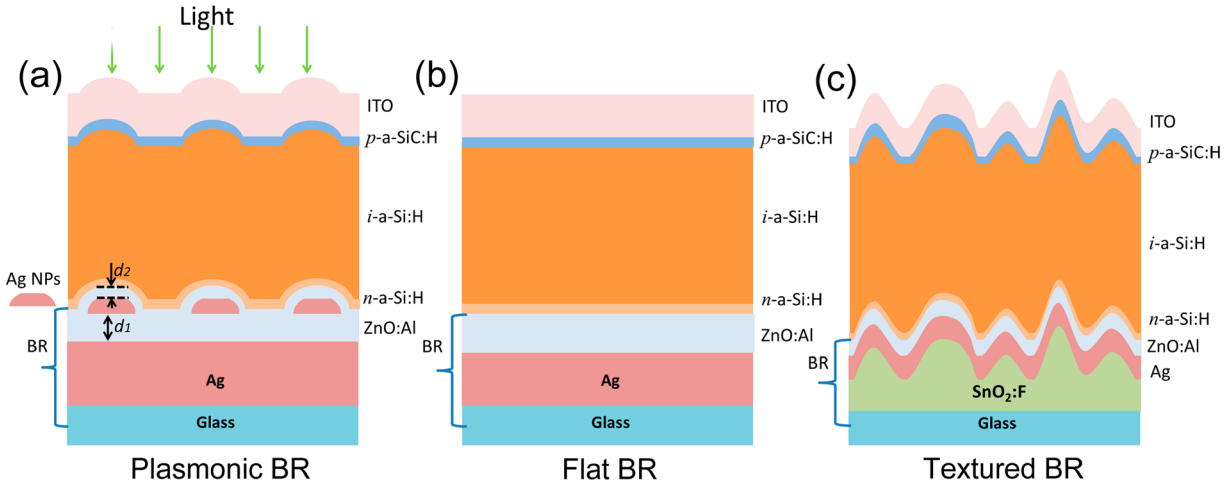

Figure 1. Schematic device structures of the n-i-p a-Si:H solar cells deposited on the plasmonic (a), flat (b), and textured (c) BRs. Light trapping of plasmonic BR is achieved by scattering of Ag NPs. The scattered light can either directly enter the silicon layers or be reflected by the planar Ag film.

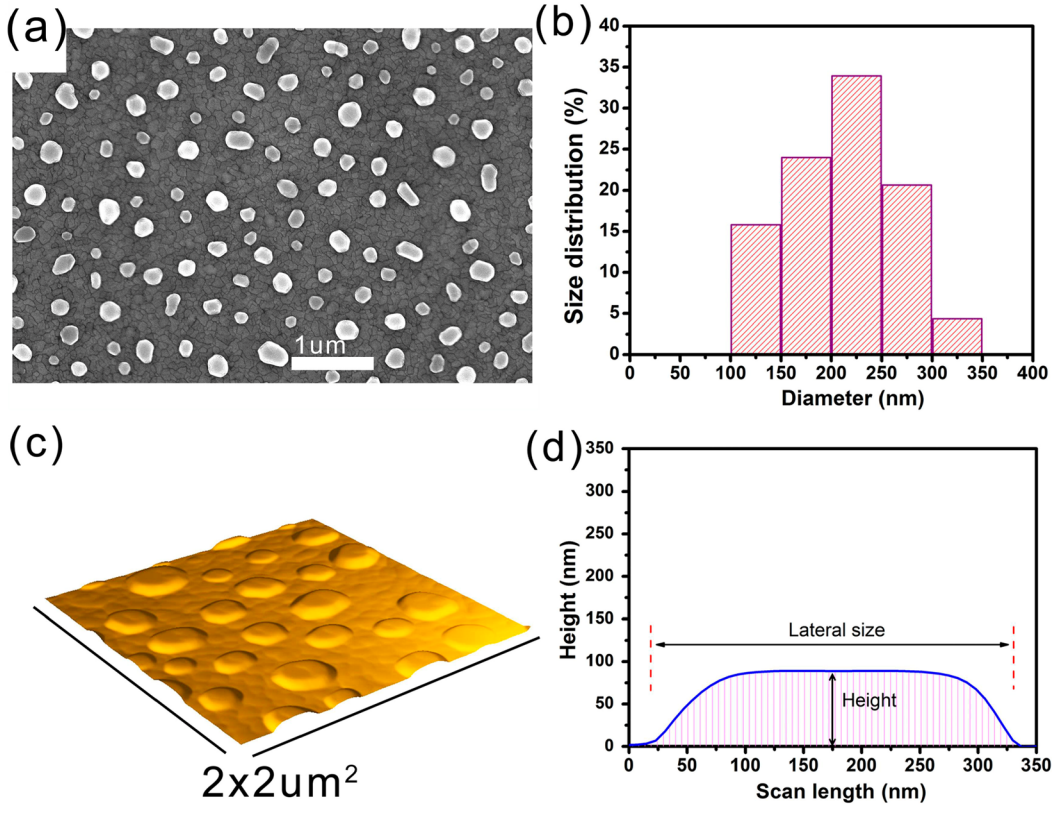

Figure 2. The morphology of flattened self-assembled Ag NPs formed at 400 °C without the AZO layer on top. SEM image (a) and size distribution (b) of Ag NPs. AFM height image 2 × 2 μm^2 (c) and typical AFM scan profile (d) of single Ag NP across the center. The diameter in panel b is calculated by $(4A/\pi)^{1/2}$, where A is the lateral area of Ag NP. The maximal height of Ag NPs in panel c is 100 nm.

state-of-the-art efficiency.[30] Asahi U-type glass is optimized for a-Si:H solar cell with an i-layer thickness around 300 nm, and it has not been demonstrated that the nanopatterned plasmonic BR can exceed Asahi glass in a-Si:H solar cells with i-layer of the optimal thickness.[24−26] In some works where high performance plasmonic a-Si:H solar cells were reported from current−voltage ($J-V$) measurements, the provided short-circuit current densities obtained from $J-V$ measurements are much higher than that from external quantum efficiency (EQE) measurements, and the reference device does not have reasonably good performance.[26,31] Thus far, there is no conclusive experimental evidence that plasmonic nanostructures can lead to comparable or even better light trapping performance to/than state-of-the-art random textures in TF-Si solar cells, even though theoretical studies indicate that plasmonic light trapping has the possibility of exceeding the classical $4n^2$ limit.[32,33]

In this Letter, we demonstrate experimentally that the plasmonic BR with random arrays of Ag NPs can provide comparable light trapping performance to state-of-the-art random textures in n-i-p a-Si:H solar cells. The conclusion is based on the comparison to high performance n-i-p a-Si:H solar

dx.doi.org/10.1021/nl301521z | Nano Lett. 2012, 12, 4070−4076

cells and state-of-the-art efficiency p-i-n solar cells deposited on Asahi VU-type glass. The Ag NPs were fabricated by self-assembling of metal island films, the most common method for fabricating random Ag NP arrays in TF-Si solar cells.[16−23,34,35] This method is a simple and cheap technique that can easily be applied to the large-area production of solar cells. However, the Ag NP arrays obtained by self-assembly in previous works always have many small (diameter <100 nm) and aggregated nanoparticles and relatively high surface coverage (>30%), that are well-known to result in undesired parasitic absorption loss and weak scattering.[34,35] The light-trapping performance can be further improved by reducing the surface coverage and by eliminating small and irregular nanoparticles. We show that increasing the annealing temperature up to 400 °C can significantly improve the morphology of Ag NPs, resulting in a surface coverage less than 20% and particle size larger than 100 nm. The obtained Ag NPs have strong scattering and low parasitic absorption.

The structure of the plasmonic BR studied in this Letter is shown in Figure 1a. It consists of a stack of glass/Ag (100 nm)/AZO (60 nm)/Ag NPs/AZO (30 nm) layers. The planar Ag layer on glass and Al-doped ZnO (AZO, ZnO:Al) layers were deposited by magnetron sputtering. The thicknesses of the two ZnO:Al layers below and above the Ag NPs are d_1 and d_2 as indicated in Figure 1a, respectively. The d_1 was chosen to completely cover the Ag film and to form Ag NPs with uniform distribution, and the d_2 was chosen to avoid the direct contact between Ag NPs and a-Si:H layer. However, here the thicknesses of the ZnO:Al layers were not fully optimized. The Ag NPs were formed by thermal evaporation of a thin Ag film with a mass thickness of 12 nm onto the Ag/AZO layers followed by one hour anneal at 400 °C in a vacuum oven. The deposition rate of the thin Ag film was less than 0.1 nm/s. Half of the substrate was covered by a mask during the deposition of the thin Ag film, and this masked area serves as the flat BR reference as shown in Figure 1b. Note that the flat BR was processed exactly the same way as the plasmonic BR except for the deposition of the 12 nm thick Ag film. The processing of plasmonic BR is prior to the deposition of silicon layers, thus the higher temperature for Ag NPs formation would not constrain the following device fabrication at lower temperature. The textured BR as presented in Figure 1c was obtained by depositing Ag/AZO layers on the Asahi VU-type glass. The textured BR was completed without further high-temperature annealing in order to keep the conformal morphology of the Asahi substrate after deposition of the Ag/AZO layers.

Figure 2a presents a scanning electron microscopy (SEM) image of self-assembled Ag NPs formed at 400 °C. This image clearly shows that Ag NPs are well-separated and have relatively round shape. The average circularity is 0.86, where circularity is calculated using $(4\pi \times \text{area})/\text{perimeter}^2$. Nanoparticles are randomly and uniformly distributed on the BR and no aggregation of nanoparticles is observed. The Ag NPs arrays have a surface coverage of around 16% and an average equivalent area diameter of 205 nm, as determined from SEM images taken in five different positions on the substrate. The size distribution given in Figure 2b shows that there are almost no particles smaller than 100 nm. Regularly shaped Ag NPs with diameter larger than 100 nm exhibit negligible parasitic absorption loss and strong localized surface plasmon scattering over a broad wavelength range of interest in TF-Si solar cells.[34−36] Atomic force microscope (AFM) images in Figure 2c,d show that Ag NPs have a flattened hemispherical shape with heights less than 100 nm. The plasmonic BR has a root-mean-square roughness of ∼22 nm, which is much smaller than that of textured BR (∼36 nm). We also note that the textured BR has a higher peak-to-peak height (maximal 260 nm) than the plasmonic BR (maximal 100 nm).

The Ag NPs formed at 400 °C here have obvious improvements compared to the Ag NPs formed at 200 °C (shown in Supporting Information Figure S1) and the reported self-assembled Ag NPs on Ag/AZO stacks used in a-Si:H or μc-Si:H solar cells and on completed thin-film crystalline Si solar cells, including more regular shape, absence of small nanoparticles, narrower size distribution, and much lower surface coverage.[16−23,34,35] These Ag NPs with more regular shape, larger size, and lower surface coverage can result in lower parasitic absorption, while Ag NPs with larger size and narrower size distribution have stronger broadband scattering over the red and infrared wavelength ranges. We attribute the improvements to the higher annealing temperature of 400 °C and favorable formation of Ag NPs on the surface of AZO. The formation of Ag NPs from a discontinuous thin Ag film under heat treatment depends on the process parameters, such as annealing temperature, thickness of Ag film, and type of substrate. When the temperature increases, the individual small size particles have higher mobility on the substrate surface, thus higher probability to agglomerate into larger particles. The higher temperature is also beneficial to form more regularly shaped particles due to increased atomic diffusion at higher temperature. We also fabricated self-assembled Ag NPs on c-Si wafer under the same processing conditions. However, the average diameter of Ag NPs is smaller (67 nm), and the surface coverage is higher (33%). This indicates that the surface properties of AZO also play a crucial role in the formation of large size and low surface coverage Ag NPs.

The function of BRs is to scatter and reflect light that has not been absorbed in a single pass, back into the absorber layers in solar cells. The light scattering properties of BRs, which are correlated with the light trapping capacity in solar cells, are usually characterized by the descriptive scattering parameters: haze in reflection (ratio of diffuse to total reflection) and the angular intensity distribution (AID) of reflected light. These parameters were measured for the three different BRs using the integrating sphere and angular-resolved transmittance/reflectance analyzer in PerkinElmer Lambda 950 spectrophotometer. Experimental details of the measurements can be found elsewhere.[37,38] As shown in Figure 3, the haze parameter of the flat BR is zero, as expected. The haze of the textured BR is high for the short wavelengths but strongly decreases with increasing wavelength above 600 nm. By contrast, the haze of the plasmonic BR formed at 400 °C is above 80% throughout the wavelength range 520−1100 nm, which is higher than the plasmonic BR formed at 200 °C (shown in Supporting Information Figure S2) and the plasmonic BR in other reports. This high haze across a broad wavelength range indicates that the plasmonic BR is not only suitable for a-Si:H solar cells (requiring light trapping up to 750 nm), but also for other TF solar cells based on lower bandgap absorbers (e.g., μc-Si:H, a-SiGe:H, and CIGS).

To obtain excellent light trapping it is desirable to scatter as much as possible light into larger angles. The haze parameter indicates the fraction of light that is scattered, but it does not indicate the angle into which this light is scattered. For this, the AID of plasmonic and textured BRs were measured in air at wavelengths λ of 600, 700, and 800 nm. The results are

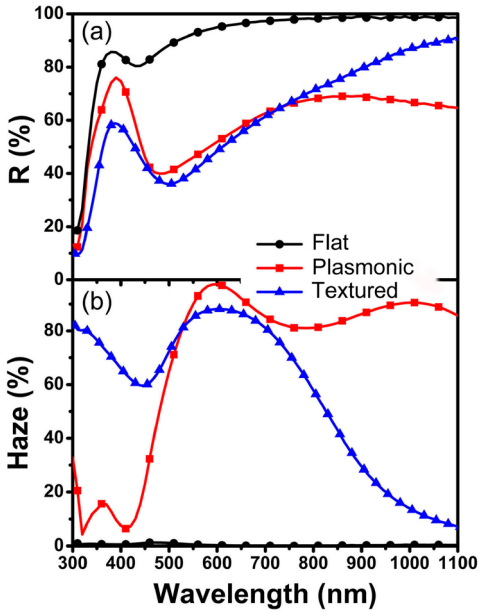

Figure 3. Total reflectance R (a) and haze in reflection (b) of flat, plasmonic, and textured BRs.

presented in Figure 4 panels a and b, respectively. The AID of the two BRs is similar in shape, and for both BRs the intensity

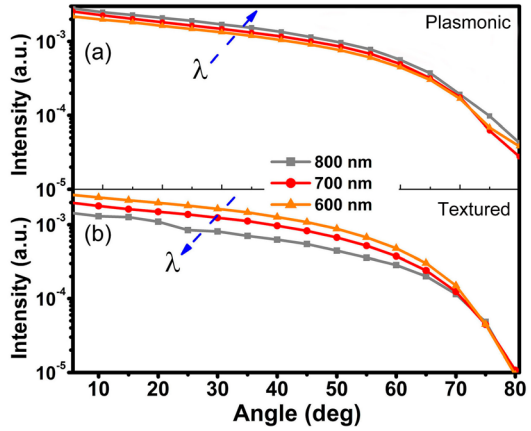

Figure 4. Angular intensity distribution of light scattered by plasmonic (a) and textured (b) back reflectors at wavelength of 600, 700, and 800 nm. The arrows indicate the trend from short to long wavelength. The scattered intensity of plasmonic BR increases with wavelength while the textured BR shows the opposite trend.

of scattered light decreases with increasing scattering angle at each wavelength. However, the intensity of the scattered light from plasmonic BR is higher than that from textured BR at each wavelength and increases with wavelength.

As shown in Figures 3 and 4, the haze and AID of the plasmonic and textured BRs reveal a significant difference in the wavelength dependence of scattering. In contrast to the conventional textured BR, the haze of the plasmonic BR does not decrease monotonically with increasing wavelength and remains high in the wavelength from 600 to 1100 nm; while the AID increases with increasing wavelength from 600 to 800 nm. The different scattering behaviors of plasmonic and textured BRs mainly are a result of differences in the fundamental scattering mechanisms. For randomly textured substrates, the scattering properties heavily rely on surface roughness, and the haze and AID reduce with increasing wavelength for a given roughness and feature size.[39] To estimate to which extent roughness-induced light scattering plays a role in the plasmonic BR, we used a validated optical model to calculate the texturing induced haze parameter.[40] Input of the morphology for the simulation is the AFM scan of the plasmonic BR shown in Figure 2c. As shown in Supporting Information Figure S3, the texturing induced haze in the plasmonic BR is much lower than the measured haze values shown in Figure 3b for wavelengths longer than 500 nm, indicating that roughness-induced light scattering does not play a significant role for light scattering in the plasmonic BR. This confirms that the plasmonic BR derives its scattering properties from the localized surface plasmon resonance of Ag NPs, a mechanism that is not directly related with surface roughness. Because of the broadband large scattering cross-section of Ag NPs, the plasmonic BR can have strong light scattering across the whole spectra for TF-Si solar cells, even though it has smooth surface features and moderate roughness as indicated in Figure 2.

For conventional light trapping based on texturing, substrates with high roughness and feature sizes comparable to the wavelength are necessary to trap long-wavelength infrared light. However, substrates with large scale surface texturing can induce defects within silicon layers grown on them and thus deteriorate photovoltaic performance.[41−43] In addition, the textured metal films suffer from parasitic surface plasmon absorption, resulting in large optical losses during multiple reflections.[44,45] As a result of these constraints, the degree of light trapping that can be achieved by textured substrates remains significantly below the theoretical limit.[46] The plasmonic BR, which has low roughness and smooth features, can provide both excellent light trapping and a good base for the growth of high quality silicon layers on top, indicating great potential to eliminate the constraints of conventional light trapping.[47,48]

To evaluate the light trapping of plasmonic BR, the n-i-p a-Si:H solar cells as shown in Figure 1 were deposited at 180 °C onto the three BRs using plasma-enhanced chemical vapor deposition. The thickness of the intrinsic absorber layers (i-layer) was 300 nm. The solar cells were completed by sputtering a 75 nm thick ITO layer (4 × 4 mm^2) as top electrode. The values of short-circuit current density (J_{sc}) reported in this work were calculated from EQE measured without bias in the range from 300 to 800 nm using the AM1.5G spectrum. This widely adopted standard method for determining the J_{sc} of lab-scale TF-Si solar cells excludes errors in the determination of J_{sc} due to spectral mismatch between the AM1.5G spectrum and light source(s) and inaccurate determination of the active area of solar cells in $J-V$ measurements. This method is essential in evaluating light trapping and its effect on device performance in solar cells. The open-circuit voltage (V_{oc}) and fill factor (FF) were determined using $J-V$ measurements under 100 mW/cm^2 illumination (AM1.5G, Oriel Newport). A well-defined 3 × 3 mm^2 hole mask was used in $J-V$ measurements to more accurately define the active area of solar cells. By using the hole mask we found that the discrepancy of J_{sc} between $J-V$ and EQE measurements is below 3%.

Figure 5a shows the EQE curves and the total device absorption (defined as unity minus the total reflectance from the device, $1 - R$) of solar cells deposited on flat and plasmonic BRs. Compared to the cell on flat BR (flat cell), a significant

dx.doi.org/10.1021/nl301521z | Nano Lett. 2012, 12, 4070−4076

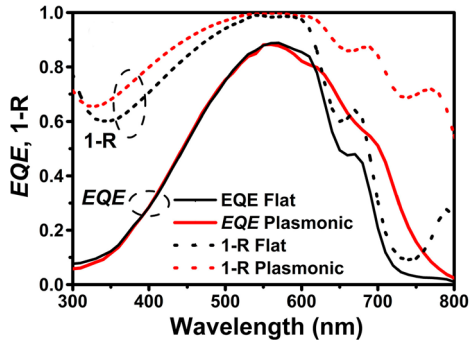

Figure 5. The EQE curves and the total device absorption (1-R) of the flat and plasmonic solar cells.

enhancement in the EQE is observed for the solar cell on the plasmonic BR (plasmonic cell) in the wavelength range 620−800 nm when compared to the flat cell. The increased EQE of the plasmonic cell clearly corresponds to the enhanced absorption of incident light in solar cells. Overall, the J_{sc} increases from 13.1 mA/cm^2 for the flat cell to 15.1 mA/cm^2 for the plasmonic cell. A gain of 2 mA/cm^2 is obtained compared with the flat cell due to effective light scattering by the Ag NPs embedded in the BR. To our knowledge, the J_{sc} of 15.1 mA/cm^2 is the highest reported J_{sc} value confirmed by EQE measurements for plasmonic a-Si:H solar cells. The plasmonic BR formed at 400 °C also resulted in higher EQE than that formed at 200 °C (EQE not shown here, J_{sc} = 14.1 mA/cm^2) at wavelengths longer than 550 nm due to the lower parasitic absorption and higher haze value, without obvious change in V_{oc} and FF.

The improvements of EQE in plasmonic TF-Si solar cells with plasmonic BR have also been reported in previous works.[20−22] The comparison of the plasmonic solar cell with a flat reference cell is interesting to demonstrate the enhancement mechanism. However, in order to evaluate the potential of plasmonic light trapping in TF-Si solar cells, it must be compared to state-of-the-art random textures. Figure 6a presents the EQE curves of a-Si:H n-i-p solar cells deposited on the plasmonic and textured BRs (textured solar cell). As we can see, the EQE curves of these two solar cells are nearly the same. In the range of 550−650 nm, the EQE of textured solar cell is slightly lower than that of plasmonic solar cell, possibly due to the plasmon absorption in the textured Ag film. Overall, the J_{sc} of plasmonic solar cell (15.1 mA/cm^2) is slightly higher than that of textured solar cell (14.8 mA/cm^2). We can conclude that the self-assembled Ag NP based plasmonic BR can at least rival a textured BR in n-i-p a-Si:H solar cells.

It is important to note that the Asahi VU-type glass is designed and optimized for use as superstrate p-i-n solar cells. Hence, for a fair comparison the EQE curve of a textured p-i-n a-Si:H solar cell deposited on the Asahi VU-type glass with 300 nm thick i-layer is included in Figure 6a as well. The $J-V$ curves of different solar cells investigated in this work are summarized in Figure 6b. The textured p-i-n solar cell with power conversion efficiency (η) of 11.1% shows significantly better blue spectral response (λ < 550 nm) than n-i-p solar cells. The main reason is that n-i-p solar cells have higher surface reflectance, higher absorption losses in the thicker p-layer, and nonoptimized i/p interfaces. Since the light with λ < 550 nm is absorbed during the first pass through the silicon layers, the spectral response in the blue range is not related to light trapping from the back reflector. To evaluate the light trapping

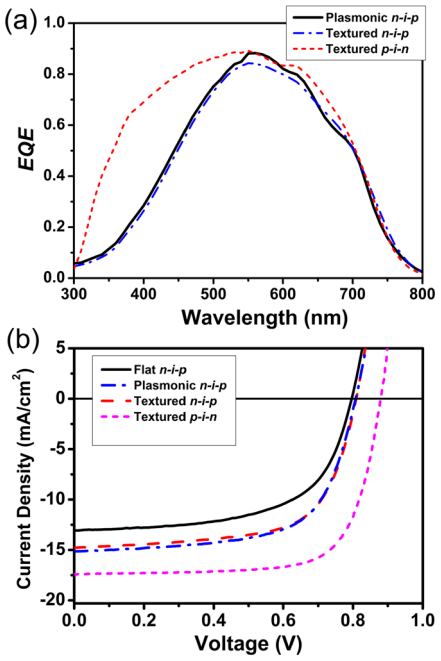

Figure 6. (a) The EQE curves of the plasmonic and textured n-i-p a-Si: solar cells and the textured p-i-n a-Si:H solar cell fabricated on the Asahi VU-type glass. (b) The $J-V$ curves of flat, plasmonic, and textured n-i-p a-Si:H solar cells, and the textured p-i-n a-Si:H solar cell.

effects, the photocurrent generated by light with λ > 550 nm ($J_{sc>550\ nm}$) can be compared. The J_{sc} and $J_{sc>550\ nm}$ of different solar cells are presented in Table 1. The $J_{sc>550\ nm}$ of the

Table 1. Characteristics of n-i-p a-Si:H Solar Cells Deposited on Flat, Plasmonic, and Textured BRs, and Textured p-i-n a-Si:H solar Cell on the Asahi VU-Type Glass

devices	V_{oc} (V)	J_{sc} (mA/cm^2)	$J_{sc>550\ nm}$ (mA/cm^2)	FF (%)	η (%)
flat n-i-p	0.80	13.1	7.4	60.3	6.3
plasmonic n-i-p	0.81	15.1	9.4	64.5	7.9
textured n-i-p	0.81	14.8	9.3	65.2	7.8
textured p-i-n	0.88	17.4	9.7	72.3	11.1

plasmonic n-i-p solar cell is only 0.3 mA/cm^2 lower than that of the textured p-i-n solar cell. This is due to a slightly lower EQE in the range of 600−700 nm maybe resulting from the destructive interference between incident and back scattered light,[17] which might be avoided by further optimization of the optical layers between n-doped layer and Ag NPs. In all, we can conclude that the plasmonic BR can lead to light trapping performance comparable to state-of-the-art random textures in a-Si:H solar cells.

The plasmonic BR has a moderate surface roughness (~22 nm) and can result in textured interfaces in solar cells that might contribute to the light trapping. Thus one could argue that the excellent light trapping of the plasmonic solar cells may be due to the roughness-induced light scattering and not mainly due to the plasmonic effects. As shown in Supporting Information Figure S3, the moderate roughness in the plasmonic BR cannot give rise to significant light scattering for wavelengths above 500 nm. The ITO/a-Si:H interface has an even lower roughness than the BR, and thus at the front side of an n-i-p solar cell the light scattering does not play an important role either. Therefore, the light trapping in

dx.doi.org/10.1021/nl301521z | Nano Lett. 2012, 12, 4070−4076

plasmonic solar cells is mainly attributed to the plasmonic light scattering, which is consistent with other works on this topic.[11,22,23,26]

To achieve high-efficiency TF-Si solar cells using plasmonic light trapping, the electrical performance (V_{oc} and FF) of the solar cells should be preserved or even improved in addition to the increase in photocurrent. Deterioration of V_{oc} and/or FF, however, was commonly reported in plasmonic TF-Si solar cells after the integration of self-assembled Ag NPs.[20−23] Here we show that the electrical performance of the plasmonic solar cell did not deteriorate. Both V_{oc} and FF of plasmonic solar cell improved compared to flat solar cell and are almost the same as textured n-i-p solar cell. After high-temperature annealing at 400 °C, the conduction of AZO film decreases and the flat solar cell had slightly lower FF (0.603) than that without high-temperature annealing (0.625); while the V_{oc} and J_{sc} did not change. Incorporation of Ag NPs into the BR can increase the conduction of AZO layer and thus lead to higher FF. On the other hand, the FF and especially V_{oc} of the n-i-p solar cells are lower in comparison to the textured p-i-n cell. The reason is that the i/p interfaces in the n-i-p devices are not optimized. Provided that the i/p interfaces are further improved, state-of-the-art efficiency above 10% can be achieved in plasmonic n-i-p solar cells.

In conclusion, we have experimentally demonstrated that self-assembled Ag NPs based plasmonic BR can provide light trapping performance comparable to state-of-the-art random textures in a-Si:H solar cells. The conclusion is based on the comparison to high performance n-i-p solar cells and high efficiency p-i-n solar cells deposited on Asahi VU-type glass. The plasmonic BR has haze in reflection above 80% in the wavelength range 520−1100 nm and can provide efficient light trapping over broad spectral range. The high performance light trapping of plasmonic BR has been demonstrated in n-i-p a-Si:H solar cells, resulting in a short circuit current as high as 15.1 mA/cm^2, without any deterioration of V_{oc} or FF. The excellent light trapping is a result of strong light scattering of Ag NPs. By self-assembling of Ag NPs at 400 °C, the high surface coverage and the formation of small and irregular particles can be avoided. Our promising results open the route to use plasmonic metal nanoparticles to obtain high efficiency and low-cost TF-Si solar cells.

■ ASSOCIATED CONTENT

Supporting Information

SEM image of Ag NPs formed at 200 °C. Total reflectance and haze in reflection of plasmonic BR formed at 200 °C. Surface texturing induced haze parameter of plasmonic BR. This material is available free of charge via the Internet at http://pubs.acs.org.

■ AUTHOR INFORMATION

Corresponding Author

*E-mail: h.tan@tudelft.nl.

Notes

The authors declare no competing financial interest.

■ ACKNOWLEDGMENTS

The authors would like to thank T. L. Temple for helpful discussion, K. Jäger for optical simulation and measurements, and G. T. Yang, S. Dobrovolskiy for technical help on the deposition of solar cells. Financial support from the Dutch STW-VIDI Grant-10782 of A.H.M.S. is gratefully acknowledged.

■ REFERENCES

(1) Kambe, M. et al. Proceedings of the 3rd World Conference on Photovoltaic Energy Conversion, Osaka, Japan, 2003.
(2) Berginski, M.; Hüpkes, J.; Schulte, M.; Schöpe, G.; Stiebig, H.; Rech, B.; Wuttig, M. *J. Appl. Phys.* **2007**, *101*, 074903.
(3) Boccard, M.; et al. *J. Photovoltaics* **2012**, DOI: 10.1109/jphotov.2011.2180514.
(4) Boccard, M.; et al. *Nano Lett.* **2012**, *12*, 1344.
(5) Yue, G. Z.; Sivec, L.; Owens, J. M.; Yan, B. J.; Yang, J.; Guha, S. *Appl. Phys. Lett.* **2009**, *95*, 263501.
(6) Yan, B. J.; Yue, G. Z.; Sivec, L.; Yang, J.; Guha, S.; Jiang, C. S. *Appl. Phys. Lett.* **2011**, *99*, 113512.
(7) Atwater, H. A.; Polman, A. *Nat. Mater.* **2010**, *9*, 205.
(8) Green, M. A.; Pillai, S. *Nat. Photon.* **2012**, *6*, 130.
(9) Polman, A. *Science* **2008**, *322*, 868.
(10) Catchpole, K. R.; et al. *MRS Bull.* **2011**, *36*, 461.
(11) Catchpole, K. R.; Polman, A. *Opt. Express* **2008**, *16*, 21793.
(12) Liz-Marzan, L. M. *Langmuir* **2006**, *22*, 32.
(13) Kelly, K. L.; Coronado, E.; Zhao, L. L.; Schatz, G. C. *J. Phys. Chem. B* **2003**, *107*, 668.
(14) Bohren, C. F.; Huffman, D. R. *Absorption and Scattering of Light by Small Particles*; Wiley: Weinheim, 2004.
(15) Kreibig, U.; Vollmer, M. *Optical Properties of Metal Clusters*; Springer: Berlin, 1995.
(16) Ouyang, Z.; Zhao, X.; Varlamov, S.; Tao, Y.; Wong, J.; Pillai, S. *Prog. Photovoltaics* **2011**, *19*, 917.
(17) Beck, F. J.; Mokkapati, S.; Polman, A.; Catchpole, K. R. *Appl. Phys. Lett.* **2010**, *96*, 033113.
(18) Beck, F. J.; Mokkapati, S.; Catchpole, K. R. *Prog. Photovoltaics* **2010**, *18*, 500.
(19) Ouyang, Z.; Pillai, S.; Beck, F. J.; Kunz, O.; Varlamov, S.; Catchpole, K. R.; Campbell, P.; Green, M. A. *Appl. Phys. Lett.* **2010**, *96*, 261109.
(20) Moulin, E.; Sukmanowski, J.; Luo, P.; Carius, R.; Royer, F. X.; Stiebig, H. *J. Non-Cryst. Solids* **2008**, *354*, 2488.
(21) Moulin, E.; Sukmanowski, J.; Schulte, M.; Gordijn, A.; Royer, F. X.; Stiebig, H. *Thin Solid Films* **2008**, *516*, 6813.
(22) Eminian, C.; Haug, F. J.; Cubero, O.; Niquille, X.; Ballif, C. *Prog. Photovoltaics.* **2011**, *19*, 260.
(23) Chantana, J.; Yang, Y. Q.; Sobajima, Y.; Sada, C.; Matsuda, A.; Okamoto, H. *J. Non-Cryst. Solids* **2012**, DOI: 10.1016/j.jnoncrysol.2011.12.038.
(24) Ferry, V. E.; Verschuuren, M. A.; Li, M. A.; Schropp, R. I.; Atwater, H. A.; Polman, A. *Appl. Phys. Lett.* **2009**, *95*, 183503.
(25) Ferry, V. E.; Verschuuren, M. A.; Li, H. B.; Verhagen, E.; Walters, R. J.; Schropp, R. E.; Atwater, H. A.; Polman, A. *Opt. Express* **2010**, *18*, A237.
(26) Ferry, V. E.; Verschuuren, M. A.; van Lare, M. C.; Schropp, R. E. I.; Atwater, H. A.; Polman, A. *Nano Lett.* **2011**, *11*, 4239.
(27) Bhattacharya, J.; Chakravarty, N.; Pattnaik, S.; Slafer, W. D.; Biswas, R.; Dalal, V. L. *Appl. Phys. Lett.* **99, 2011**, 131114.
(28) Paetzold, U. W.; Moulin, E.; Michaelis, D.; Bottler, W.; Wachter, C.; Hagemann, V.; Meier, M.; Carius, R.; Rau, U. *Appl. Phys. Lett.* **2011**, *99*, 181105.
(29) Paetzold, U. W.; Moulin, E.; Pieters, B. E.; Carius, R.; Rau, U. *Opt. Express* **2011**, *19*, A1219.
(30) Battaglia, C.; et al. *ACS Nano* **2012**, *6*, 2790.
(31) Chen, X.; Jia, B. H.; Saha, J. K.; Cai, B. Y.; Stokes, N.; Qiao, Q.; Wang, Y. Q.; Shi, Z. R.; Gu, M. *Nano Lett.* **2012**, *12*, 2187.
(32) Callahan, D. M.; Munday, J. N.; Atwater, H. A. *Nano Lett.* **2012**, *12*, 214.
(33) Yu, Z.; Raman, A.; Fan, S. *Proc. Natl. Acad. Sci. U.S.A.* **2010**, *107*, 17491.
(34) Santbergen, R.; Temple, T. L.; Liang, R.; Smets, A.; van Swaaij, R. M.; Zeman, M. *J. Opt.* **2012**, *14*, 024010.

(35) Temple, T. L.; Mahanama, G. K.; Reehal, H. S.; Bagnall, D. M. *Sol. Energy Mater. Sol. Cells* **2009**, *93*, 1978.
(36) Temple, T. L.; Bagnall, D. M. *Prog. Photovoltaics* **2012**, DOI: 10.1002/pip.1237.
(37) Jäger, K.; Isabella, O.; Zhao, L.; Zeman, M. *Phys. Status Solidi C* **2010**, *7*, 945.
(38) Jäger, K.; Isabella, O.; van Swaaij, R. M.; Zeman, M. *Meas. Sci. Technol.* **2011**, *22*, 105601.
(39) Zeman, M.; van Swaaij, R. M.; Metselaar, J. W.; Schropp, R. E. *J. Appl. Phys.* **2000**, *88*, 6436.
(40) Jäger, K.; Fischer, M.; van Swaaij, R. M.; Zeman, M. *J. Appl. Phys.* **2012**, *111*, 083108.
(41) Söderström, T.; Haug, F. J.; Terrazzoni-Daudrix, V.; Ballif, C. *J. Appl. Phys.* **2008**, *103*, 114509.
(42) Python, M.; Vallat-Sauvain, E.; Bailat, J.; Donine, D.; Fesquet, L.; Shah, A.; Ballif, C. *J. Non-Cryst. Solids.* **2008**, *354*, 2258.
(43) Boccard, M.; Cuony, P.; Despeisse, M.; Domine, D.; Feltrin, A.; Wyrsch, N.; Ballif, C. *Sol. Energy Mater. Sol. Cells* **2011**, *95*, 195.
(44) Springer, J.; Poruba, A.; Mullerova, L.; Vanecek, M.; Kluth, O.; Rech, B. *J. Appl. Phys.* **2004**, *95*, 1427.
(45) Haug, F. J.; Soderstrom, T.; Cubero, O.; Terrazzoni-Daudrix, V.; Ballif, C. *J. Appl. Phys.* **2008**, *104*, 064509.
(46) Yablonovitch, E. *J. Opt. Soc. Am.* **1982**, *72*, 899.
(47) Sai, H.; Kanamori, Y.; Kondo, M. *Appl. Phys. Lett.* **2011**, *98*, 113502.
(48) Söderström, T.; Bugnon, G.; Haug, F. J.; Nicolay, S.; Ballif, C. *Sol. Energy. Mater. Sol. Cells* **2012**, *101*, 193.